Mizukami, S., Watanabe, S., **Kikuchi, K.**	Development of ratiometric fluorescent probes for phosphatases by using a pK_a switching mechanism.	*Chembiochem*	48	1465-1468	2009
Yamaguchi, S., Miura, C., **Kikuchi, K.**, Celino, F. T., Agusa, T., Tanabe, S., Miura, T.	Zinc is an Essential Trace Element for Spermatogenesis.	*Proc. Natl. Acad. Sci. U. S. A.*	106	10859-10864	2009
Kikuchi, K., Hashimoto, S., Mizukami, S., Nagano, T.	Anion sensor-based ratiometric peptide probe for protein kinase activity.	*Org. Lett.*	11	2732-2735	2009
Mizukami, S., Okada, S., Kimura, S., **Kikuchi, K.**	Design and synthesis of coumarin-based Zn^{2+} probes for ratiometric fluorescence imaging.	*Inorg. Chem.*	48	7630-7638	2009
Hori, Y., Ueno, H., Mizukami, S., **Kikuchi, K.**	Photoactive yellow protein-based protein labeling system with turn-on fluorescence intensity.	*J. Am. Chem. Soc.*	131	16610-16111	2009
Hori, Y., Egashira, Y., Kamiura, R., **Kikuchi, K.**	Noncovalent-Interaction-Promoted Ligation for Protein Labeling.	*Chembiochem*	11	646-648	2010
Okada, S., Mizukami, S., **Kikuchi, K.**	Application of Stimuli-Responsive Polymer for Development of Novel MRI Probes.	*Chembiochem*	1	785-787	2010
Watanabe, S., Mizukami, S., Hori, Y., **Kikuchi, K.**	Multicolor Protein Labeling in Living Cells Using Mutant β-Lactamase-tag Technology.	*Bioconjug. Chem.*	21	2320-2326	2010
Sadhu, K.K., Mizukami, S., Watanabe, S., **Kikuchi, K.**	Turn-on Fluorescence Switch Involving Aggregation and Elimination Processes for β-Lactamase-Tag.	*Chem. Commun.*	46	7403-7405	2010
Mizukami, S., Hosoda, M., Satake, T., Okada, S., Hori, Y., Furuta, T., **Kikuchi, K.**	Photocontrolled Compound Release System Using Caged Antimicrobial Peptide.	*J. Am. Chem. Soc*	132	9524-9525	2010
Yoshimura, A.,	Cell Surface Protein Labeling with Luminescent Nanoparticles	*Chembiochem*	12	1031-1034	2011

Mizukami, S., Hori, Y., Watanabe, S., **Kikuchi, K.**	via Biotinylation Using Mutant β-Lactamase-tag Technology.				
Sadhu, K.K., Mizukami, S., Watanabe, S., **Kikuchi, K.**	Sequential Ordering Among Multicolor Fluorophores for Protein Labeling Facility via Aggregation-elimination Based β-Lactam Probes.	*Mol. BioSyst.*	7	1766-1772	2011
Mizukami, S., Matsushita, H., Takikawa, R., Sugihara, F., Shirakawa, M., **Kikuchi, K.**	^{19}F MRI Detection of β-Galactosidase Activity for Imaging of Gene Expression,	*Chem. Sci.*	2	1151-1155	2011
Sadhu, K. S., Mizukami, S., Hori, Y., **Kikuchi, K.**	Switching Modulation for protein labeling with activatable fluorescent probes.	*Chembiochem.*	12	1299-1308	2011
Watanabe, S., Mizukami, S., Akimoto, Y., Hori, Y., **Kikuchi, K.**	Intracellular Protein Labeling with Prodrug-Like Probes Using a Mutant β-Lactamase Tag.	*Chem. Eur. J.*	17	8342-8349	2011
Mizukami, S., Yamamoto, T., Yoshimura, A., Watanabe, S., **Kikuchi, K.**	Covalent Protein Labeling with a LanthanideComplex and its Application to Photoluminescence Lifetime-based Multicolor.	*Angew. Chem. Int. Ed.*	50	8750-8752	2011
Kowada, T., Kikuta, J., Kubo, A., Ishii, M., Maeda, H., Mizukami, S., **Kikuchi, K.**	In Vivo Fluorescence Imaging of Bone-Resorbing Osteoclasts	*J. Am. Chem. Soc.*	133	17772-17776	2011
Mizukami, S., Watanabe, S., Akimoto, Y., **Kikuchi, K.**	No-Wash Protein Labeling Designed Fluorogenic Probes and Application to Real-Time	*J. Am. Chem. Soc.*	134	1623-1629	2012
Okada, S., Mizukami, S., **Kikuchi, K.**	Switchable MRI contrast agents based on morphological changes of pH-responsive polymers	*Bioorg. Med. Chem.*	20	769-774	2012
Terai, T., **Kikuchi, K.**, Urano, Y., Kojima, H., Nagano, T.	A long-lived luminescent probe to sensitively detect arylamine N-acetyltransferase (NAT) activity of cells.	*Chem. Commun.*,	48	2234-2236	2012

Sadhu, K., Mizukami, S., Lanam, C. R., **Kikuchi, K.**	Fluorogenic Protein Labeling through Photoinduced Electron Transfer-Based BL-tag Technology,	*Chem. Asian. J.*	7	272-276	2012
Hori, Y., Nakaki, K., Sato, M., Mizukami, S., **Kikuchi, K.**	Development of Protein-Labeling Probes with Redesigned Fluorogenic Switch Based on Intramolecular Association for No-wash Live-cell Imaging	*Angew. Chem. Int. Ed.*		In press	2012
Iwaya, N., Akiyama, K., Goda, N., Tenno, T., Fujiwara, Y., Hamada, D., Ikura, T., Shirakawa, M., Hiroaki, H.	Effect of Ca^{2+} on microtubule severing enzyme katanin p60; insight into the substrate dependent activation mechanism.	*FEBS J.*	279(7)	1339-1352	2012
Fukuchi, S., Sakamoto, S., Nobe, Y., Murakami, D. S., Amemiya, T., Hosoda, K., Koike, R. Hiroaki, H., Ota, M.	IDEAL - Intrinsically Disordered proteins with Extensive Annotations and Literature.	*Nucleic Acids Research (database issue),*	40(1)	D507-511	2012
Hiroaki, H., Umetsu, Y., Hoshi, M., Nabeshima, Y. Kohda, D.	A Simplified Recipe for Assigning Amide NMR Signals Using Combinatorial ^{14}N Amino Acid Inverse-Labeling.	*J Structural Functional Genomics.,*	12(3)	167-174	2011
Tsuruta, T., Umetsu, Y., Iwaya, N., Taniguchi, R., Goda, N., Tenno, T., Kuwahara, Y., Hiroaki, H.,	^{1}H, ^{13}C, and ^{15}N resonance assignment of the SPFH domain of human stomatin.	*Biomol. NMR Assign*	6(1)	23-25	2011
Hasegawa, J., Tokuda, E., Tenno, T., Tsujita, K., Sawai, H., Hiroaki, H., Takenawa, T. Itoh, T.	SH3YL1 regulates dorsal ruffle formation by a novel phosphoinositide- binding domain.	*J Cell Biol*	193(5)	901-916	2011
Fujiwara, Y., Fujiwara, K., Goda, N., Iwaya, N., Tenno, T., Shirakawa, M., Hiroaki, H.	Structure and function of the N-terminal nucleolin binding domain of nuclear Valocin containing protein like 2 (NVL2) harboring a nucleolar localization signal.	*J Biol Chem*	286(24)	21732-21741	2011
Umetsu, Y., Taniguchi, R.,	^{1}H, ^{13}C, and ^{15}N resonance assignment of the first PDZ	Biomol. NMR Assign.		In press	2011

Satomura, R., Goda, N., Ikegami, T., Furuse, M., Hiroaki, H.	domain of mouse ZO-1.				
Umetsu, Y., Tenno, T., Goda, N., Shirakawa, M., Ikegami, T., Hiroaki, H.	Structural difference of vasoactive intestinal peptide (VIP) in two distinct membrane mimicking conditions.	*BBA-Proteins Proteomics*	1814	724-730	2011
Motono, C., Nakata, J., Koike, R., Shimizu, K., Shirota, M., Amemiya, T., Tomii, K., Nagano, N., Sakaya, N., Misoo, K., Sato, M., Kidera, A., Hiroaki, H., Shirai, T., Kinoshita, K., Noguchi, T., Ota, M.	SAHG, a comprehensive database of predicted structures of all human proteins.	Nucleic Acids Res.	39(suppl 1)	D487-D493	2010
Iwaya, N., Kuwahara, Y., Fujiwara, Y., Goda, N., Tenno, T., Akiyama, K., Mase, S., Tochio, H., Ikegami, T., Shirakawa, M., Hiroaki, H.	A common substrate recognition mode conserved between katanin p60 and VPS4 governs microtubule severing and membrane skeleton reorganization.	J Biol. Chem.	285	16822-16829	2010
Jee, J., Mizuno, T., Kamada, K., Tochio, H., Chiba, Y., Yanagi, K., Yasuda, G., Hiroaki, H., Hanaoka, F., Shirakawa, M.	Structure and mutagenesis studies of the C-terminal region of licensing factor Cdt1 enable the identification of key residues for binding to replicative helicase Mcm proteins.	J Biol. Chem.	285	15931-15940	2010
Fukushima F, Nakao K, Shinoe T, Fukaya M, Muramatsu S, Sakimura K, Kataoka H, Mori H, Watanabe M, Manabe M and	Ablation of NMDA receptors enhances the excitability of hippocampal CA3 neurons.	PLoS ONE	4(1)	e3993	2009

Mishima M					
Kuratomi S, Ohmori Y, Ito M, Shimazaki K, Muramatsu S, Mizukami H, Uosaki H, Yamashita JK, Arai Y, Kuwahara K and Takano M	The cardiac pacemaker-specific channel Hcn4 is a direct transcriptional target of MEF2.	Cardiovasc Res	83(4)	682-687	2009
Muramatsu S, Okuno T, Suzuki Y, Nakayama T, Kakiuchi T, Takino N, Iida A, Ono F, Terao K, Inoue N, Nakano I, Kondo Y and Tsukada H	Multi-tracer assessment of dopamine function after transplantation of embryonic stem cell-derived neural stem cells in a primate model of Parkinson's disease.	Synapse	63	541-548	2009
Tanaka Y, Ikeda T, Masuda S, Shibata H, Takeuchi K, Komura M, Iwanaka T, Muramatsu S, Kondo Y, Takahashi K, Yamanaka S and Hanazono Y	ERas is expressed in primate embryonic stem cells but not related to tumorigenesis.	Cell Transplant	18(4)	381-389	2009
Okuno T, Nakayama T, Konishi N, Michibata H, Wakimoto K, Suzuki Y, Nito S, Inaba T, Nakano I, Muramatsu S, Takano M, Kondo	Self-contained induction of neurons from human embryoniv stem cells.	PLoS ONE	4	e6318	2009

Y, and Inoue N					
Ito T, Yamamoto S, Hayashi T, Kodera M, Mizukami H, Ozawa K and Muramatsu S	A convenient enzyme-linked immunosorbent assay for rapid screening of anti-adeno-associated virus neutralising antibodies.	Ann Clin Biochem	46(Pt 6)	508-510	2009
Noguchi A, Matsumura S, Dezawa M, Tada M, Yanazawa M, Ito A, Akioka M, Kikuchi S, Sto M, Ideno S, Noda M, Fukunari A, Muramatsu, S, Itokazu Y, Sato K, Takahashi H, Teplow DB, Nabeshima Y, Kakita A, Imahori K and Hoshi M	Isolation and characterization of patient-derived, toxic, high-mass amyloid β -protein (A β) assembly from Alzheimer's disease brains.	J Biol Chem	284(47)	32895-905	2009
Kadkhodaei B, Ito T, Joodmardi E, Mattsson B, Rouillard C, Carta M, Muramatsu S, Ichinose C, Nomura T, Chambon P, Metzger D, Larsson N, Lindqvist E, Olson L, Bjorklund A and Ichinose H	Nurr1 is required for maintenance of maturing and adult midbrain dopamine neurons.	J Neurosci	29(50)	15923-15932	2009
Krzyżosiak A, Szyszka-Niagolov M, Wietrzych M, Gobaille S, Muramatsu S and	Retinoid X receptor gamma control of motivated behaviours involves dopaminergic signalling in mice.	Neuron	66(6)	908-920	2010

Krężel W.					
Muramatsu S, Okuno T, Suzuki Y, Nakayama T, Kakiuchi T, Takino N, Iida A, Ono F, Terao K, Inoue N, Nakano I, Kondo Y and Tsukada H	A phase I study of aromatic L-amino acid decarboxylase gene therapy for Parkinson's disease.	Mol Ther	18(9)	731-1735	2010
Muramatsu S, Asari S, Fujimoto K, Ozawa K and Nakano I	Gene therapy for Parkinson's disease. Strategies for the local production of dopamine.	Gene Therapy & Regulation	5(1)	57-65	2010
Muramatsu S	The current status of gene therapy for Parkinson's disease,	Ann Neurosci	17(2)	92-95	2010
Asari S, Fujimoto K, Miyauchi A, Sato T, Nakano I and Muramatsu S	Subregional 6-[18F]fluoro-L-m-tyrosine uptake in the striatum in Parkinson's disease.	BMC Neurol	-	11-35	2011
Tokuoka H, Muramatsu S, Ichinose C, Sakane H, Kojima M, Aso Y, Nomura T, Metzger D and Ichinose H	Compensatory regulation of dopamine after ablation of the tyrosine hydroxylase gene in the nigrostriatal projection.	J Biol Chem	286(50)	43549-43558	2011
Miyamoto M, Miyamoto T, Iwanami M, Muramatsu S, Asari S, Nakano I and Hirata K	Preclinical substantia nigra dysfunction in rapid eye movement sleep behaviour disorder.	Sleep Med	13(1)	102-106	2011
Jin D, Muramatsu S, Shimizu N, Yokoyama S, Hirai	Dopamine release via the vacuolar ATPase V0 sector c-subunit, confirmed in N18 neuroblastoma	Neurochem Int	-	-	In Press

H, Yamada K, Liu HX, Higashida C, Hashii M, Higashida A, Asano M, Ohkuma S and Higashida H	cells, results in behavioral recovery in hemiparkinsonian mice.				

III.　研究成果の刊行物・別刷り

THE JOURNAL OF BIOLOGICAL CHEMISTRY VOL. 286, NO. 13, pp. 11555–11562, April 1, 2011

Two Distinct Amyloid β-Protein (Aβ) Assembly Pathways Leading to Oligomers and Fibrils Identified by Combined Fluorescence Correlation Spectroscopy, Morphology, and Toxicity Analyses*[S]

Received for publication, September 6, 2010, and in revised form, January 23, 2011 Published, JBC Papers in Press, February 3, 2011, DOI 10.1074/jbc.M110.181313

Satoko Matsumura,[a1] Keiko Shinoda,[b1] Mayumi Yamada,[a1] Satoshi Yokojima,[b] Masafumi Inoue,[c] Takayuki Ohnishi,[c] Tetsuya Shimada,[d] Kazuya Kikuchi,[e] Dai Masui,[d] Shigeki Hashimoto,[f] Michio Sato,[a] Akane Ito,[a] Manami Akioka,[a] Shinsuke Takagi,[d] Yoshihiro Nakamura,[g] Kiyokazu Nemoto,[h] Yutaka Hasegawa,[i] Hisayoshi Takamoto,[i] Haruo Inoue,[d] Shinichiro Nakamura,[b] Yo-ichi Nabeshima,[c] David B. Teplow,[j] Masataka Kinjo,[k] and Minako Hoshi[a,c2]

From the [a]Mitsubishi Kagaku Institute of Life Sciences, Tokyo 194-8511, Japan, [b]Mitsubishi Chemical Group Science and Technology Research Center, Inc., Yokohama 227-8502, Japan, [c]Kyoto University, Kyoto 606-8501, Japan, [d]Tokyo Metropolitan University, Tokyo 192-0397, Japan, [e]Osaka University, Osaka 565-0871, Japan, [f]Tokyo University of Science, Hokkaido 049-3514, Japan, [g]Nagoya Institute of Technology, Aichi 466-8555, Japan, [h]Chibadai Inohana Innovation Plaza, Chiba 260-0856, Japan, [i]Hamamatsu Photonics K.K., Shizuoka 438-0193, Japan, [j]University of California, Los Angeles, California 90095, and [k]Hokkaido University, Sapporo 001-0021, Japan

Nonfibrillar assemblies of amyloid β-protein (Aβ) are considered to play primary roles in Alzheimer disease (AD). Elucidating the assembly pathways of these specific aggregates is essential for understanding disease pathogenesis and developing knowledge-based therapies. However, these assemblies cannot be monitored *in vivo*, and there has been no reliable *in vitro* monitoring method at low protein concentration. We have developed a highly sensitive *in vitro* monitoring method using fluorescence correlation spectroscopy (FCS) combined with transmission electron microscopy (TEM) and toxicity assays. Using Aβ labeled at the N terminus or Lys^{16}, we uncovered two distinct assembly pathways. One leads to highly toxic 10–15-nm spherical Aβ assemblies, termed amylospheroids (ASPDs). The other leads to fibrils. The first step in ASPD formation is trimerization. ASPDs of ~330 kDa in mass form from these trimers after 5 h of slow rotation. Up to at least 24 h, ASPDs remain the dominant structures in assembly reactions. Neurotoxicity studies reveal that the most toxic ASPDs are ~128 kDa (~32-mers). In contrast, fibrillogenesis begins with dimer formation and then proceeds to formation of 15–40-nm spherical intermediates, from which fibrils originate after 15 h. Unlike ASPD formation, the Lys^{16}-labeled peptide disturbed fibril formation because the $Aβ^{16-20}$ region is critical for this final step. These differences in the assembly pathways clearly indicated that ASPDs are not fibril precursors. The method we have developed should facilitate identifying Aβ assembly steps at which inhibition may be beneficial.

Conversion of disease-specific amyloid proteins from the native forms into fibrillar assemblies is a common feature of a wide range of human pathologies, including neurodegenerative diseases such as AD,[3] Parkinson disease, prion diseases, and the polyglutamine diseases (1–5). On the other hand, smaller, nonfibrillar assemblies, which might be early precursors in fibrillogenesis, have recently been considered to be more proximate mediators of neurotoxicity (1–5). However, it is unclear whether these originate from a linear process or a series of parallel processes involving different intermediates. Thus, ordering the assembly pathway(s) is essential for understanding disease pathogenesis and developing rational therapeutics, as inhibiting inappropriate step(s) could increase the level of the toxic assemblies (2, 5).

In AD, various forms of toxic Aβ assemblies, ranging in mass from dimers to multimers of ~1 MDa, have been reported (6–14). These assemblies may play the key role in AD pathogenesis by causing synaptic impairment (12, 13, 15–17). Indeed, Aβ dimers that induce synaptic impairment and not neuronal loss have been reported to be isolated from AD brains (18). In contrast, the molecular natures of the Aβ assemblies that directly cause neuronal loss in human AD remain to be elucidated. Because neuronal loss causes cognitive deterioration in AD patients (19), we sought to isolate such Aβ assemblies *in vivo*. As a first step, we prepared highly toxic 10–15-nm spherical Aβ assemblies termed ASPDs using an *in vitro* assembly

* This work was supported by grants from the Ministry of Health, Labor and Welfare (Research on Nanotechnical Medical) (to M. H.), Special Coordination Funds for Promoting Science and Technology from the Ministry of Education, Culture, Sports, Science, and Technology (to K. K. and M. H.), the New Energy and Industrial Technology Development Organization (Translational Research Promotion Project) (to M. H.), and the Jim Easton Consortium for Alzheimer's Drug Discovery and Biomarkers (to D. B. T.).

[S] The on-line version of this article (available at http://www.jbc.org) contains supplemental "Experimental Procedures," equations, Table S1, Figs. S1–S8, and additional references.

[1] These authors contributed equally to the work.

[2] To whom correspondence should be addressed: Yoshidakonoecho, Sakyo-ku, Kyoto 606-8501, Japan. Tel.: 81-75-7534683; Fax: 81-75-7534676; E-mail: minhoshi@lmls.med.kyoto-u.ac.jp.

[3] The abbreviations used are: AD, Alzheimer disease; Aβ, amyloid β-protein; FCS, fluorescence correlation spectroscopy; TEM, transmission electron microscopy; ASPD, amylospheroid; ADDLs, Aβ-diffusible ligands; TMR, tetramethylrhodamine; ha, hamster monoclonal; PBS, Dulbecco's phosphate-buffered saline without Ca^{2+} and Mg^{2+}; IP, immunoprecipitation.

system (10). ASPDs are not fibril intermediates because they are not incorporated into mature fibrils and continue to exist after fibril formation ceases (5, 10). They also differ from protofibrils and Aβ-derived diffusible ligands (ADDLs) in morphology and size (10) (see reviews in Refs. 5 and 20)). Recently, we have produced ASPD-specific antibodies and used them to selectively immunoisolate highly neurotoxic ASPDs from human AD brains (21), strengthening the hypothesis that ASPDs are effectors of neurodegeneration *in situ* in humans. We also found that ASPD concentration correlated with the pathological severity of AD (21). These findings suggest that native ASPDs might be a candidate for Aβ assemblies that directly cause neuronal loss in human AD brains. The immunoreactivity profile of ASPD-specific antibodies in comparison to that of anti-Aβ antibodies or of an anti-oligomer A11 antibody suggests that ASPDs are structurally distinct from dimers, ADDLs, and A11-reactive entities (21). Taken together, data extant suggest that distinct types of Aβ assemblies, with distinct neurotoxic activities, exist in the AD brain. Therefore, elucidation of the assembly state-neurotoxicity relationships of these assemblies is important for understanding AD pathogenesis.

Here, we use combined FCS, TEM, and toxicity analyses to address these issues and to provide a highly sensitive and reliable method for *in situ* monitoring of the assembly process. At present, the assembly process cannot be monitored directly *in vivo* and much higher sensitivity is required for reliably monitoring *in vitro* formation of nonfibrillar Aβ assemblies, which occurs at low protein concentration (5, 20, 22–25). Our approach should therefore be useful in studies of other amyloid proteins.

FCS involves autocorrelation of fluctuations of fluorescence intensity, which gives the average number and average diffusion time (*i.e.* molecular size) of fluorescent molecules as they diffuse through an illuminated volume (26). We employed FCS because FCS provides the highest sensitivity for detecting small assemblies in dilute solutions among available analytical techniques (small angle x-ray diffraction, ultracentrifugation, laser light scattering, etc.). In addition, FCS does not require physical separation of metastable assemblies, and its noninvasive character allows monitoring without perturbation of monomer-nonfibrillar assembly-fibril equilibria (27–29). Although FCS has been employed to detect Aβ aggregates in cerebrospinal fluid of AD patients (30) and the formation of large (>10^4 kDa) fibrillar assemblies from $A\beta^{1-40}$ *in vitro* (29, 31), little is known about the formation of neurotoxic nonfibrillar Aβ assemblies. Here, by using combined FCS, TEM, and toxicity analyses, we uncovered two distinct assembly pathways, one leading to ASPDs and the other to fibrils. We also determined the mass (128 ± 44 kDa) and height (7.2 ± 2.6 nm) of the most toxic ASPDs. The observed differences in the assembly pathways clearly indicated that ASPDs are not fibril precuorsors.

EXPERIMENTAL PROCEDURES

Materials—ASPD-specific antibodies, a rabbit polyclonal rpASD1 ($K_d \approx 5$ pM) and a hamster monoclonal haASD1 ($K_d \approx 0.5$ pM), have been produced in our laboratory and recognize epitopes distinct from those present on dimers, A11 antibody-reactive 12-mers, or fibrils (21). The characteristics of these ASPD tertiary structure-dependent antibodies are summarized in supplemental Table S1.

Sample Preparations—Fluorescent probes, $A\beta^{1-40}$ site-specifically labeled with tetramethylrhodamine (TMR) either at the N terminus (NTR) or Lys16 (K16TR), were synthesized (supplemental "Experimental Procedures"). ASPDs were prepared *in vitro* from 50 μM solutions of $A\beta^{1-42}$ (with or without 0.1 μM NTR or K16TR; a probe ratio of 1/500) in F12 buffer without riboflavine, L-glutamine, and phenol red by slowly rotating the solutions at 4 °C for 16.5 h (10). Their quality was confirmed by dot blotting, TEM, and toxicity assays. Spherical assemblies 10–15 nm in diameter, with rare fibril-like structures, were usually produced as major components (10). Fibrils were prepared from 100 μM solutions of $A\beta^{1-40}$ (with or without 0.1 μM NTR or K16TR; a probe ratio of 1/1000) in 0.5× Dulbecco's phosphate-buffered saline without Ca^{2+} and Mg^{2+} (PBS) at pH 3.5 by slowly rotating the solutions at 4 °C for 2 days. Fibrils without ASPDs were detected by TEM. Aβ concentration of each preparation was determined by quantitative amino acid analysis (Waters AccQ-Tag system) (10).

FCS—FCS was performed with a confocal volume element of 0.3 femtoliters using a preproduction prototype apparatus (Hamamatsu Photonics K.K.). The fluorescence intensity fluctuations were detected using a photomultiplier tube, and the autocorrelation function was calculated using a digital correlator (Fig. 1*A*; see also supplemental "Experimental Procedures"). Each sample (20 μl) was measured at room temperature for 3 s × 10 times using free rhodamine 6G (479 Da in mass, 2.8×10^{-10} m^2 s^{-1} in the diffusion coefficient (*D*)) or Alexa Fluor 532 C5 maleimide (813 Da, 2.8×10^{-10} m^2 s^{-1}) as reference dyes.

FCS Data Evaluation—At the onset of the assembly process, Aβ solutions mainly contain rapidly diffusing Aβ assemblies ranging in mass from monomers to trimers. Some other assemblies may also be present, but their concentrations are unpredictable. Therefore, the constrained regularization program CONTIN (32, 33), combined with least-squares fitting, was utilized to determine the distribution of the diffusion times so that the mass of the rapidly diffusing Aβ assemblies fitted the dimer/trimer range (8~15 kDa), without any prior assumption about the number of the assembly types in solutions. From the determined distributions, the relative abundance and diffusion time of each assembly were calculated. By comparing the diffusion time of each assembly with that of reference dyes with known mass and diffusion coefficient, the mass (for spherical assemblies such as ASPDs) or the diffusion coefficient (*D*) (for nonspherical assemblies such as fibrils) was determined (supplemental Fig. S3). The details are described in the supplemental "Experimental Procedures."

In FCS, the contribution of each component to the correlation curve is related to both its relative abundance and brightness (34). If all components have equal brightness, the relative abundance of each assembly can be obtained directly from the distribution of assembly diffusion time. This is true for ASPDs and early fibril intermediates, but not for fibrils containing more than one fluorophore. In the latter case, a rough estimate of the relative abundance of the fibrils was obtained from the distribution of the diffusion time (for details, see "*In Situ* Monitoring of Fibril Formation" under "Results"). To confirm the estimates thus obtained,

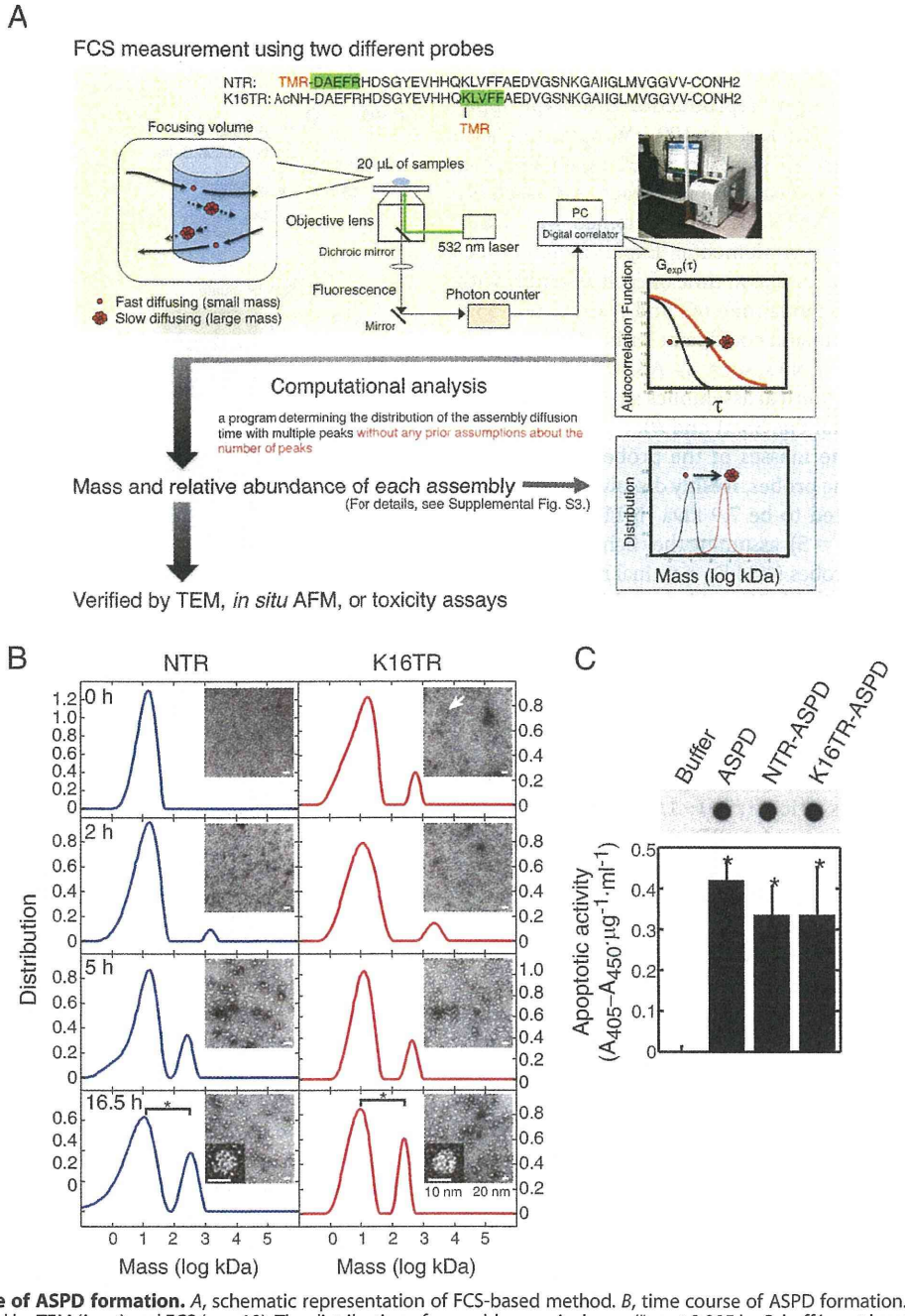

FIGURE 1. **Time course of ASPD formation.** *A*, schematic representation of FCS-based method. *B*, time course of ASPD formation. At the indicated time, aliquots were examined by TEM (*inset*) and FCS ($n = 10$). The distribution of assembly mass is shown (*, $p < 0.005$ by Scheffé post hoc test compared with the fast-diffusing assembly). Each distribution is normalized so that the total area becomes 1 (as described under "Experimental Procedures"). An *arrow* in TEM data indicates not-yet-dissolved amorphous aggregates. *C*, characterization of ASPDs formed with or without probes in dot blotting (1 pmol/dot using 0.04 μg/ml ASPD-specific rpASD1 antibody) or specific apoptotic activity against rat primary septal neuronal cultures, determined by monitoring cytoplasmic histone-associated DNA fragments, and normalized by the amount of Aβ present (mean ± S.D.; Games-Howell post hoc test. *, $p < 0.005$, $n = 6$; see supplemental "Experimental Procedures").

mature fibrils were separated in the retentate fractions of 0.1-μm filters (confirmed using TEM), and their amount was directly obtained from the fluorescence count using a fluorometer (Twinkle LB970; Berthold Technologies GmbH).

Other Methods—Immunoprecipitation (IP), TEM, fluid-phase imaging of ASPDs by atomic force microscopy, toxicity assays, and statistics are described in the supplemental "Experimental Procedures."

RESULTS

Fluorescent Probes for FCS Measurements and Program for FCS Analysis—To monitor ASPD formation by FCS, we chemically synthesized fluorescent probes by labeling TMR site-specifically either at the N terminus (termed NTR) or at Lys^{16} (termed K16TR) of $A\beta^{1-40}$ (Fig. 1*A*). We consider TMR labeling at these sites to minimally affect ASPD formation because

excess $A\beta^{1-5}$ (DAEFR) or $A\beta^{16-20}$ (KLVFF) had no effect on ASPD formation (supplemental Fig. S1), suggesting that amino acid residues around $A\beta^{1-5}$ or $A\beta^{16-20}$ are not involved in ASPD formation.

FCS was performed using a preproduction prototype apparatus (Hamamatsu Photonics K.K.) at 100 μW optimum laser output power (supplemental Fig. S2). From FCS data, the relative abundance (%) and diffusion time of each Aβ assembly were obtained using CONTIN (32, 33) combined with least-squares fitting (Fig. 1*A*; see supplemental "Experimental Procedures"). By comparing the diffusion time of each assembly with those of reference dyes (rhodamine 6G and Alexa Fluor 532) with known mass and diffusion coefficient, either the assembly mass (for spherical assemblies such as ASPDs) or diffusion coefficient (*D*) (for nonspherical assemblies such as fibrils) was determined (supplemental Fig. S3, *A* and *B*).

First, we examined the masses of the probes by FCS. The average mass values of the probes, freshly dissolved at 0.1 μM in 0.5× PBS, were calculated to be 7.9 kDa (NTR) and 8.6 kDa (K16TR), respectively ($n = 5$), assuming they behave as spherical structures. Thus, these probes (4.8 kDa nominal mass) behave as dimers, like unlabeled $A\beta^{1-40}$ (35), and should be available for incorporation into ASPDs during assembly. The result validates the accuracy of our FCS-based analytical method.

In Situ Monitoring of ASPD Formation—Next, we examined whether ASPDs were formed in the presence of the probes. Consistent with our study using unlabeled $A\beta^{1-42}$ (10), TEM revealed the formation of 10–15-nm ASPDs in the presence of NTR or K16TR at various ratios (1/500~1/10 of total Aβ; 16.5 h in Fig. 1*B*, *inset*). FCS detected ASPD-sized structures in the range of 100–1000 kDa (16.5 h in Fig. 1*B*) (10) even at a 1/500 probe ratio. NTR- or K16TR-labeled ASPDs were indistinguishable from unlabeled ASPDs in immunoreactivity to anti-ASPD antibodies and in neurotoxicity to rat primary neuronal cultures (Fig. 1*C*). Accordingly, we set the probe ratio at 1/500 for subsequent experiments. Because the mass of ASPDs does not exceed 669 kDa (*i.e.* ~148-mer) (21), at 1/500 probe ratio, assemblies will contain a maximum of one fluorophore per assembly, so they will have equal brightness. This means that we can obtain the relative abundance of each assembly directly from the distribution of assembly diffusion time determined by CONTIN (see "Experimental Procedures").

We then followed time-dependent changes in Aβ assembly state simultaneously using TEM and FCS (Fig. 1*A*). As shown previously (10), during up to 2 h of slow rotation, TEM detected few structures except for occasional amorphous structure (Fig. 1*B*, *arrow* at 0 h in *inset*). During this initial phase of ASPD formation, up to 2 h, Aβ trimers (12.7 ± 1.8 kDa, 92%, $n = 8$) predominated (Fig. 1*B*). This means the first step in ASPD formation involves trimerization. Besides trimers, FCS also detected small amounts of large assemblies with varying mass and relative abundance (for time 0, 10^2~10^7 kDa in mass, 8.4 ± 11%; for 2 h, 10^2~10^4 kDa, 11.3 ± 7.2%; $n = 8$) (supplemental Fig. S4). This is consistent with the observation of low numbers of cloud-like uranyl acetate staining structures (*dotted line* in supplemental Fig. S4, *inset*), distinct from the staining of buffer-derived salts, up to 2 h in TEM. We speculate that these large species are metastable and therefore may be destroyed during

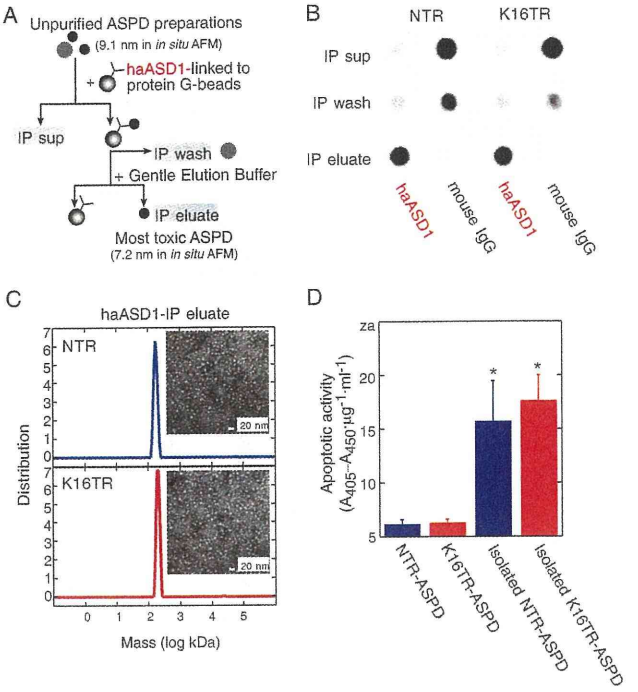

FIGURE 2. **Isolation of the most toxic ASPD fraction.** *A*, method for IP. *B*, dot blotting (using 0.04 μg/ml rpASD1) of IP supernatant (*sup*), wash, and eluate fractions. *C*, the isolated ASPDs in haASD1-IP eluates examined by TEM (*Inset*) and FCS ($n = 10$). The distribution is normalized as in Fig. 1*B*. ASPDs were undetectable in mouse IgG-IP eluates using TEM or FCS (data not shown). *D*, specific apoptotic activities of the isolated ASPDs and unpurified ASPDs were examined as in Fig. 1*C* (mean ± S.D.; Games-Howell post hoc test; *, $p < 0.001$, $n = 6$).

sample preparation for TEM. Although it is unclear whether these species are intermediates of ASPDs, it is noteworthy that neither the cloud-like structures nor the large species with such variety in mass and relative abundance were absent at the onset of fibril formation (see "*In Situ* Monitoring of Fibril Formation"; see Fig. 3). After that, ASPDs appeared at 5 h of slow rotation. At this time, 5–20-nm spherical structures, mainly 10–15-nm ASPD-sized spheres, were observed (Fig. 1*B*, *inset*). ASPDs remained as the dominant structures from 5 h until at least 24 h (Fig. 1*B*, *inset*). In accordance with TEM observations, FCS detected an ASPD-sized assembly of 10^2 ~ 10^3 kDa at 5 h, and its amount was increased at 16.5 h (Fig. 1*B* and supplemental Fig. S4). Its mass was 330 ± 58 kDa (24 ± 7.7%, $n = 5$), in good agreement with that of ASPDs (~158–669 kDa) previously estimated from glycerol-gradient sedimentation assays (5, 10). Thus, we conclude we could monitor ASPD formation continuously and quantitatively using FCS. The two probes gave essentially identical results (Fig. 1*B*).

Mass and Height of Isolated ASPDs—We recently produced ASPD-specific antibodies (supplemental Table S1) (21) and used them to selectively immunoisolate ASPDs from AD brain extracts without affecting ASPD structure or neurotoxicity (21). With this method (Fig. 2*A*), we immunoisolated the most toxic fraction of ASPDs from unpurified ASPD preparations and determined the mass using our FCS method. Large amounts of 10–15-nm ASPDs were detected only in IP eluates of a monoclonal ASPD-specific haASD1 antibody, whereas ASPDs were undetectable in IP eluates of normal mouse IgG

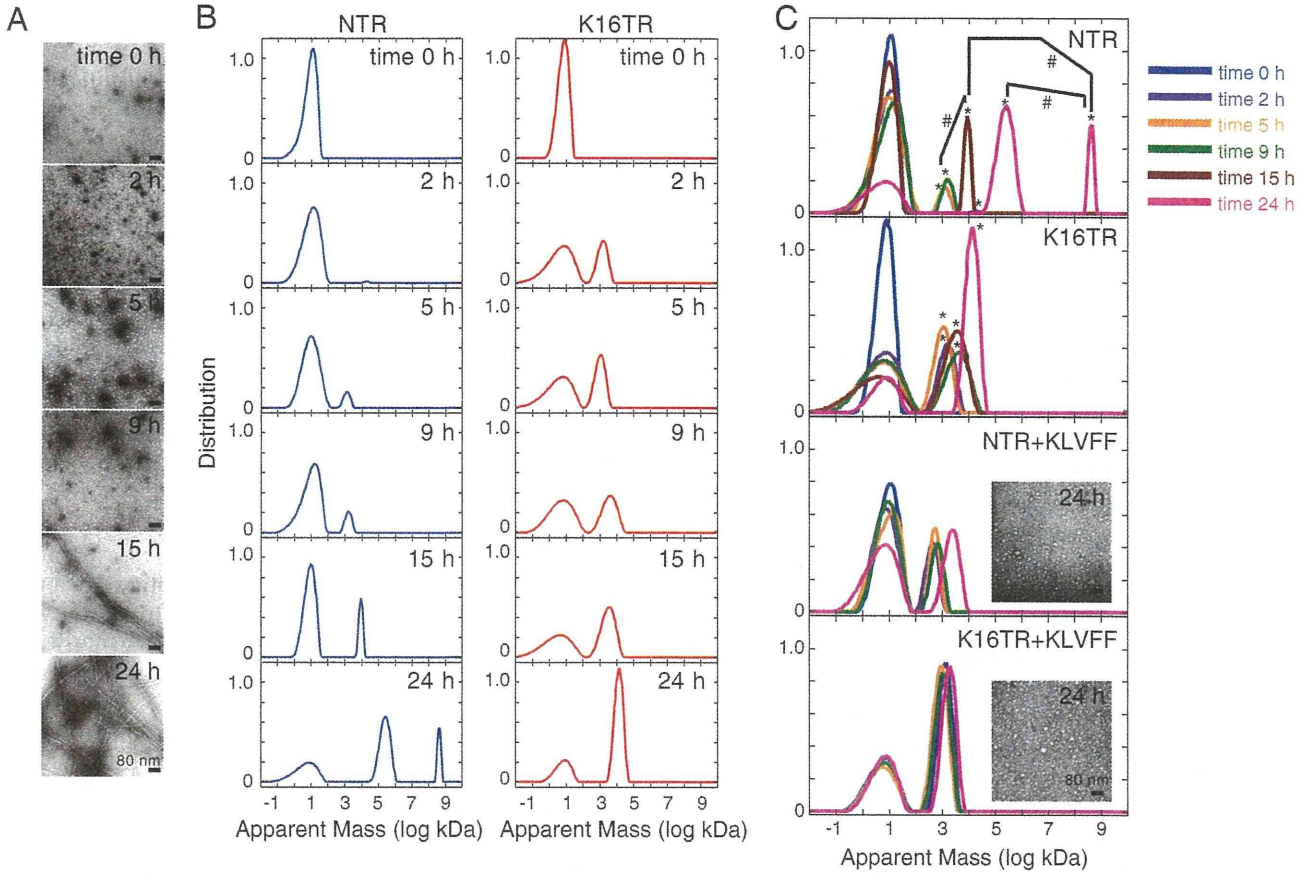

FIGURE 3. **Time course of fibril formation.** *A* and *B*, fibrils were formed from 100 μM solutions of $A\beta^{1-40}$ with 0.1 μM NTR or K16TR at pH 3.5. At the indicated time, aliquots were examined by TEM (*A*) and FCS ($n = 5$) (*B*). As fibrillogenesis proceeded essentially in the same way with or without probes, representative TEM images of fibrils with NTR are shown. The normalized distribution of apparent assembly mass (see supplemental Fig. S7 for diffusion coefficient) is shown, as in Fig. 1*B*. *C*, at the onset of fibril formation, a 10-fold molar excess of $A\beta^{16-20}$ (KLVFF) was added to the $A\beta^{1-40}$ solutions, and analyses using TEM (*inset*) and FCS were performed as above (*, $p < 0.005$ by Scheffé post hoc test compared with the fast-diffusing assembly corresponding to dimers; #, $p < 0.005$ by Scheffé post hoc test). The probability distribution is normalized as in Fig. 1*B*.

(Fig. 2, *B* and *C*, *inset*). In accordance with this, 97% of the fluorescent species in haASD1-IP eluates detected by FCS was ASPD-sized assemblies of 128 ± 44 kDa ($n = 6$) (Fig. 2*C*). The IP process mostly eliminated Aβ dimers (9.4 ± 4.0 kDa) (Fig. 2*C*), which had been a major component before IP (76%, $n = 5$, 16.5 h in Fig. 1*B*). The neurotoxicity of the purified ASPDs to rat primary neuronal cultures was >10 times greater than that of the unpurified ASPD preparations (Fig. 2*D* and supplemental Fig. S5). These data collectively indicated that the most toxic ASPDs were concentrated by the IP procedures. Their mass estimated from FCS analysis was in good agreement with our previous sedimentation results, which indicated that the highest toxicity exists in the fraction at the migration position of 158-kDa aldolase (10, 21). The most toxic ASPDs (128 ± 44 kDa; ~32-mers) were smaller in mass than the unpurified ASPDs (330 ± 58 kDa; compare Fig. 2*C* with 16.5 h in Fig. 1*B*). Consistent with these data, *in situ* atomic force microscopy imaging in physiological solutions (10) revealed that the average height of the most toxic ASPDs (7.2 ± 2.6 nm, 94%, supplemental Fig. S6) was smaller than that of the unpurified ASPDs (9.1 ± 2.0 nm (10)). We thus have succeeded in determining the mass and height of the most toxic ASPDs for the first time.

In Situ Monitoring of Fibril Formation—We next monitored fibril formation (supplemental Fig. S3B). We used acidic solutions because fibrils are well formed from 100 μM $A\beta^{1-40}$ at pH 3.5 (36), whereas ASPDs are hardly formed (24 h in Fig. 3*A*). Because fibrils contain higher numbers of Aβ monomers than ASPDs (10), we set the probe ratio for fibrils at 1/1000. As with ASPDs, if all components have equal brightness, the relative abundance of each assembly can be obtained from the distribution of assembly diffusion times determined by CONTIN. This is true for early assemblies before 15 h (< 5,000 kDa) that will contain a maximum of one fluorophore per assembly at 1/1000 probe ratio. However, this might not be the case for late stage assemblies (after 15 h), which include very large assemblies (probably mature fibrils) with more than one fluorophore per assembly (Fig. 3); here, as the contribution of a component to the FCS correlation curve scales with the brightness squared, the fraction of brighter component will be overestimated (34). The problem is that the number of fluorophores per fibril (*i.e.* fibril brightness) cannot be determined, because fibrils exist over a wide mass range. Furthermore, fibril formation may alter the fluorophore quantum yield (37). Therefore, a rough estimate of fibril amount was obtained from the distribution of

assembly diffusion times and was confirmed by separating the mature fibrils in retentate fractions on 0.1-μm filters and by directly measuring their fluorescence.

As with ASPDs, time-dependent changes in Aβ assembly state were monitored simultaneously using TEM and FCS (Fig. 3). At the onset of slow rotation, amorphous structures incorporating small globular structures (<3 nm) were occasionally detected in trace amounts with TEM (Fig. 3*A*). At 2 h, as reported previously (14), 15–40-nm spherical intermediates (larger than 10–15-nm ASPDs) appeared and increased until 5 h (Fig. 3*A*). Then, with the formation of short fibril-like structures, these spherical intermediates decreased at 9 h and were no longer detectable at 15 h (Fig. 3*A*). Mature fibrils appeared at 15 h, and their amount was markedly increased at 24 h. Subsequently, these fibrils grew into meshwork-like or bundled fibrils (Fig. 3*A*). These morphological changes generally occurred in this sequence, irrespective of the presence or absence of probes, although the size and morphology of mature fibrils varied somewhat among preparations.

TEM observations confirmed that the presence of either probe at 1/1000 did not affect overall fibrillogenesis (Fig. 3*A*). However, the two probes gave different FCS results at 24 h (Fig. 3*B*). To illustrate the time-dependent size changes, we show the diffusion coefficient (supplemental Fig. S7) and apparent mass (Fig. 3) of each structure both for spherical structures (5 h in Fig. 3*A*) and nonspherical structures (15 and 24 h in Fig. 3*A*). Unlike ASPD formation, at the onset of fibril formation, Aβ dimers (9.2 ± 1.7 kDa, 85% at time 0, $1.4 \pm 0.2 \times 10^{-10}$ m^2s^{-1}, $n = 6$) were the dominant species (Fig. 3*B*), which decreased to 41% at 24 h. Consistent with the TEM results, large aggregates of ~10^3 kDa were occasionally detected by FCS at time 0. At 2 h, Aβ assemblies of ~2910 kDa in average mass appeared and remained detectable up to 9 h (29%, $2.2 \pm 0.7 \times 10^{-11}$ m^2s^{-1}, $n = 18$; see NTR and K16TR in upper two panels in Fig. 3*C*). Their average masses likely correspond to the 15–40-nm spherical intermediates (5 h in Fig. 3*A*). At 15 h, consistent with their disappearance in TEM (Fig. 3*A*), they were hardly detectable with FCS, and other Aβ assemblies of 5.4×10^3 kDa in apparent mass, a slightly larger than the 15–40-nm intermediates, appeared (roughly 38%, $1.6 \pm 0.4 \times 10^{-11}$ m^2 s^{-1}, $n = 6$; Fig. 3*B*). Although the two probes, NTR and K16TR, behaved similarly up to 15 h, they gave different results at 24 h. NTR detected two kinds of Aβ assemblies, a very large Aβ assembly of 1.2×10^5 kDa in apparent mass (roughly 45%, $0.7 \pm 0.4 \times 10^{-11}$ m^2 s^{-1}, $n = 3$) and another much larger Aβ assembly of 3.9×10^9 kDa in apparent mass (roughly 7%, $1.9 \pm 0.9 \times 10^{-13}$ m^2 s^{-1}, $n = 3$) (Fig. 3*B*). However, K16TR only detected the former very large Aβ assembly of 1.4×10^4 kDa in apparent mass (roughly 64%, $1.3 \pm 0.7 \times 10^{-11}$ m^2 s^{-1}, $n = 3$), but failed to detect the latter huge Aβ assembly (Fig. 3*B*). As described above, to confirm the estimates at 15 and 24 h, the fibril amount was directly obtained by filtration using 0.1-μm filters, followed by counting of fluorescence intensity. The fibril amounts in the 0.10-μm retentates were 29 ± 7% (NTR) and 36 ± 3% (K16TR) at 15 h, and 74 ± 7% (NTR) and 61 ± 6% (K16TR) at 24 h ($n = 5$; supplemental Fig. S8). These data seem consistent with the FCS results (38% at 15 h ($n = 6$) and 52% for NTR and 64% for K16TR at 24 h ($n = 3$)) (Fig. 3*B*), suggesting that the fibril amount can be estimated using FCS.

As for the difference between NTR and K16TR at 24 h, we speculate that TMR introduced at Lys^{16} disturbed incorporation of K16TR into mature fibrils, because the 16–20 region of Aβ is known to be critical for Aβ self-association and subsequent fibril formation (38). To examine this hypothesis, we added excess $Aβ^{16-20}$ (KLVFF) at the onset of Aβ assembly. In TEM and FCS analyses (Fig. 3*C*), 15–40-nm spherical intermediates that had disappeared at 15 h without $Aβ^{16-20}$ (Fig. 3, *A* and *B*) remained as the dominant structures in the presence of excess $Aβ^{16-20}$, up to 24 h (Fig. 3*C*, *inset*). NTR and K16TR both detected these spherical intermediates even at 24 h (2280 kDa, for $2.2 \pm 0.2 \times 10^{-11}$ m^2 s^{-1} for NTR, 3370 kDa, $1.9 \pm 0.3 \times 10^{-11}$ m^2 s^{-1} for K16TR, $n = 3$, Fig. 3*C* and supplemental Fig. S7). This result indicated that $Aβ^{16-20}$ did not prevent assembly of Aβ dimers into spherical intermediates but blocked conversion of the latter into fibrils.

DISCUSSION

A large body of evidence supports the hypothesis that nonfibrillar Aβ assemblies play causative roles in AD (3, 5, 20, 22–25). Accordingly, Aβ assemblies other than fibrils have recently been proposed as therapeutic targets (39). However, Aβ monomers develop into various nonfibrillar Aβ assemblies differing in size and toxicity, which might represent distinct structural variants (5, 20, 24, 40). It is not clear whether and how these different types of assemblies are related to each other or indeed how they contribute to AD pathogenesis.

To elucidate the neurotoxic molecular entities responsible for AD pathogenesis, several approaches have been employed to reveal the formation of nonfibrillar Aβ assemblies *in vitro*. For example, studies using HPLC multiangle laser light scattering analysis (41) determined the size of certain forms of nonfibrillar Aβ assemblies. Studies using a UV-cross-linking method (42) or limited proteolysis with mass analysis (43) elucidated the roles of various amino acid residues in the formation of nonfibrillar Aβ assemblies, and solid-state NMR analysis revealed conformational changes in the early stage of fibril formation (14). Interestingly, in the case of cross-linked Aβ oligomers, higher order oligomers have stronger neurotoxicity (44). These studies and others together suggest that assembly may not be a linear process but may be the result of a series of multiple processes involving intermediates from side paths (5). However, these approaches could not follow the continuous changes of assembly state in solution and the assembly state-neurotoxicity relationship largely remained to be uncovered.

Here, we have developed a highly sensitive *in vitro* monitoring method using combined FCS, TEM, and toxicity analyses. Applying this method to Aβ labeled with TMR at the N terminus or Lys^{16}, we uncovered two distinct assembly pathways, one leading to highly toxic 10–15-nm spherical Aβ assemblies termed ASPDs (10), which we showed to exist *in vivo* (21), and the other to fibrils. The first step in ASPD formation is trimerization. ASPDs of ~330 kDa in mass originate from these trimers after 5 h of slow rotation (Fig. 1*B*). At least until 24 h, ASPDs remained the dominant structures in these reactions. Previously, we reported that ASPDs are formed from 50 μM

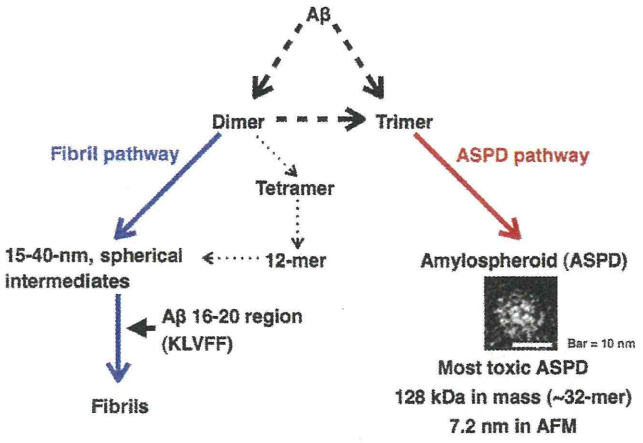

FIGURE 4. **Two distinct Aβ assembly pathways, one leading to ASPDs (*red*) and the other to fibrils (*blue*).** The first step in ASPDs formation is trimerization (Fig. 1), whereas the pathway to fibrils begins with dimers, which further assemble into 15–40-nm spherical intermediates, eventually leading to fibrils (Fig. 3*B*). The $A\beta^{16-20}$ region is critical for intermediate conversion into fibrils (Fig. 3*C*), but not for ASPD formation (supplemental Fig. S1). Although the assembly pathway to 12-mers is unknown, tetramers might serve as a precursor of 12-mers (45); if this is so, the assembly pathway to 12-mers (*dotted line*) differs at the initial step from that of ASPDs.

$A\beta^{1-42}$ within 14 h during slow rotation (10). With the present method, we could thus more easily and accurately monitor ASPD formation, as well as detect ASPDs themselves. Indeed, we found that the most toxic ASPDs are ~128 kDa in mass (~32-mers) (Fig. 2 and supplemental Fig. S5) and are 7.2 nm in height (supplemental Fig. S6).

Our previous data have strongly suggested that ASPDs have a distinct tertiary structure from other assemblies (21). Therefore, we were interested in whether or not ASPDs share building blocks with these assemblies. With respect to dimers (18), we found that they clearly are not building blocks *per se* because the initial step in ASPD formation is trimerization (Fig. 1*B*). We could not detect 12-mers during ASPD formation (supplemental Fig. S4). This suggests that 12-mers are not precursors of ASPDs. Although the assembly pathway to 12-mers is unknown, ion mobility-mass spectrometry studies have shown that tetramers might serve as a precursor of 12-mers (45), indicating that the assembly pathway to 12-mers may differ at the initial step from that of ASPDs. These results collectively demonstrated that the assembly pathway to ASPDs is distinct from those leading to dimers and to 12-mers. We propose a scheme of the assembly pathways based on these findings (Fig. 4).

In contrast to ASPD formation, the first step leading to fibrils consists in the assembly of Aβ monomers into dimers, which further assemble into 15–40-nm spherical intermediates, eventually leading to fibrils (blue arrows in Fig. 4). Although the $A\beta^{16-20}$ region is not involved in ASPD formation (supplemental Fig. S1), we found that this region is critical for conversion of the spherical intermediates to fibrils because probe labeling at Lys^{16} was found to disturb fibrillogenesis (Fig. 3*C*). Excess amounts of the $A\beta^{16-20}$ (KLVFF) peptide in fibril formation reactions inhibited the process, supporting this conclusion (Fig. 3*C*). As for 12-mers, we could not detect them as a single peak during fibril formation (Fig. 3*B*), which suggests that even though 12-mer formation appears to begin with dimer formation (45), the 12-mers do not directly serve as a primary fibril precursor (Fig. 4). This view is consistent with other studies showing that 12-mers are semistable structures that do not readily form fibrils (12), and it would likely take a slow transformation process for them to rearrange into fibrils (45). Of relevance to the role of dimers in fibrillogenesis are data recently published by the Walsh and co-workers (46) that show that dimers themselves are inert with respect to neurotoxicity but that their further assembly produces higher order toxic prefibrillar assemblies. Consistently with this, dimers in AD brains have been reported to be contained in amyloid cores as insoluble reservoirs that do not readily dissociate (18).

Previously, we have shown that both $A\beta^{1-40}$ and $A\beta^{1-42}$ form ASPDs of ~158–669 kDa in sedimentation assays, and among them, the highest toxicity exists in the fraction at the migration position of 158 kDa (aldolase) (10, 21). Epitope analysis of ASPD-specific antibodies has also suggested that $A\beta^{1-40}$ and $A\beta^{1-42}$ ASPDs share the same tertiary structures because essentially the same results are obtained in inhibition studies of ASPD-specific antibodies through the binding to either $A\beta^{1-40}$ or $A\beta^{1-42}$ ASPDs of pentapeptides derived from Aβ (21). However, there exists a critical difference between $A\beta^{1-40}$ and $A\beta^{1-42}$ in the rate and speed of ASPD formation. $A\beta^{1-42}$ ASPDs are formed more rapidly, after 5 h of incubation, and in greater quantities (24%). They induce neurodegeneration at lower concentration (~0.35 nM) and exhibit ~100-fold higher toxicity than $A\beta^{1-40}$ ASPDs (10). In contrast, $A\beta^{1-40}$ forms ASPDs after 3 days of incubation, but in lesser amounts (5% on average) than does $A\beta^{1-42}$ (10). These observations are consistent with the general consensus that $A\beta^{1-42}$ is more toxic than $A\beta^{1-40}$. Interestingly, we found that the first step to $A\beta^{1-40}$ ASPDs also consists in the assembly of $A\beta^{1-40}$ monomers into trimers (12.7 ± 0.4 kDa, 93%, $n = 4$; data not shown). Although $A\beta^{1-40}$ seemingly behaves as trimers in FCS, we speculate that, probably because of the absence of the stabilizing influence of the hydrophobic carboxyl terminus, $A\beta^{1-40}$ trimers are more unstable than $A\beta^{1-42}$ trimers and therefore less likely to form ASPDs. This view is supported by other studies using different analytical methods, including SDS-PAGE, ion mobility-mass spectroscopy, and size exclusion spectroscopy (45, 47, 48), all of which have indicated the absence of trimers/tetramers in $A\beta^{1-40}$. Certain differences in the initial folded structures and properties between $A\beta^{1-40}$ and $A\beta^{1-42}$ might be reflected in the differences in their ability to form higher order assemblies (45, 47, 48). Although the conformation adopted by Aβ within the nonfibrillar Aβ assemblies is not known, a β-hairpin has recently been reported to be a building block of toxic Aβ assemblies; this was established by engineering a double-cysteine mutant in which the β-hairpin is stabilized by an intramolecular disulfide bond (48). Notably, the double-cysteine mutant $A\beta^{1-42}$ has been reported to form SDS-stable dimers/trimers, particularly trimers, which were absent in the mutant $A\beta^{1-40}$ (48). As a result, the mutant $A\beta^{1-42}$ forms highly neurotoxic, A11-negative, β-sheet-enriched assemblies of ~100 kDa (apparent mass on size exclusion chromatography) more readily than the mutant $A\beta^{1-40}$ does (48). Such conformational difference in $A\beta^{1-40}$ and $A\beta^{1-42}$ monomers might be reflected in the differences of ASPD formation. It is also possible that con-

formational differences in the initial monomer state might cause differences in dimer or trimer formation, leading to the distinct assembly pathways observed here. Further analysis, *e.g.* with NMR, is needed to elucidate the molecular mechanism of the differences.

To conclude, the observed differences in the assembly pathways clearly indicated that ASPDs are not fibril precursors, in accordance with the fact that ASPDs continued to exist after mature fibril formation without being incorporated into fibrils (5, 10). Our data also support the idea that the assembly pathway to ASPDs is different from the pathways leading to fibrils and to oligomers such as dimers and 12-mers (5, 10). As has also been suggested by others (45, 47, 48), our data further support the view that distinct assembly pathways lead to formation of assemblies with distinct tertiary structures (Fig. 4). We have thus discerned the different pathways by employing the combined FCS method, which should facilitate identifying the assembly steps where inhibition might be beneficial. This method should also be useful to find biological molecules or chemical factors that inhibit formation of these nonfibrillar Aβ assemblies and offers the potential for developing therapeutic agents based on this mechanistic understanding.

Acknowledgments—We thank A. Noguchi (Mitsubishi Kagaku Institute of Life Sciences) for technical help with IP; Dr. M. Noda (Mitsubishi Tanabe Pharma Corp.) for haASD1 antibody; Drs. Y. Kobayashi, H. Yokozawa, and K. Kanda (Mitsubishi Chemical Group Science and Technology Research Center) for technical help with atomic force microscopy and for computational set-up, respectively; and Drs. Y. Ishii (University of Illinois) and Y. Fujiyoshi (Kyoto University) for valuable discussions.

REFERENCES

1. Selkoe, D. J. (1991) *Neuron* **6,** 487–498
2. Ross, C. A., and Poirier, M. A. (2005) *Nat. Rev. Mol. Cell Biol.* **6,** 891–898
3. Lansbury, P. T., and Lashuel, H. A. (2006) *Nature* **443,** 774–779
4. Chiti, F., and Dobson, C. M. (2009) *Nat. Chem. Biol.* **5,** 15–22
5. Roychaudhuri, R., Yang, M., Hoshi, M. M., and Teplow, D. B. (2009) *J. Biol. Chem.* **284,** 4749–4753
6. Levine, H., 3rd (1995) *Neurobiol. Aging* **16,** 755–764
7. Podlisny, M. B., Ostaszewski, B. L., Squazzo, S. L., Koo, E. H., Rydell, R. E., Teplow, D. B., and Selkoe, D. J. (1995) *J. Biol. Chem.* **270,** 9564–9570
8. Walsh, D. M., Lomakin, A., Benedek, G. B., Condron, M. M., and Teplow, D. B. (1997) *J. Biol. Chem.* **272,** 22364–22372
9. Lambert, M. P., Barlow, A. K., Chromy, B. A., Edwards, C., Freed, R., Liosatos, M., Morgan, T. E., Rozovsky, I., Trommer, B., Viola, K. L., Wals, P., Zhang, C., Finch, C. E., Krafft, G. A., and Klein, W. L. (1998) *Proc. Natl. Acad. Sci. U.S.A.* **95,** 6448–6453
10. Hoshi, M., Sato, M., Matsumoto, S., Noguchi, A., Yasutake, K., Yoshida, N., and Sato, K. (2003) *Proc. Natl. Acad. Sci. U.S.A.* **100,** 6370–6375
11. Kayed, R., Head, E., Thompson, J. L., McIntire, T. M., Milton, S. C., Cotman, C. W., and Glabe, C. G. (2003) *Science* **300,** 486–489
12. Barghorn, S., Nimmrich, V., Striebinger, A., Krantz, C., Keller, P., Janson, B., Bahr, M., Schmidt, M., Bitner, R. S., Harlan, J., Barlow, E., Ebert, U., and Hillen, H. (2005) *J. Neurochem.* **95,** 834–847
13. Lesné, S., Koh, M. T., Kotilinek, L., Kayed, R., Glabe, C. G., Yang, A., Gallagher, M., and Ashe, K. H. (2006) *Nature* **440,** 352–357
14. Chimon, S., Shaibat, M. A., Jones, C. R., Calero, D. C., Aizezi, B., and Ishii, Y. (2007) *Nat. Struct. Mol. Biol.* **14,** 1157–1164
15. Deshpande, A., Mina, E., Glabe, C., and Busciglio, J. (2006) *J. Neurosci.* **26,** 6011–6018
16. Lacor, P. N., Buniel, M. C., Furlow, P. W., Clemente, A. S., Velasco, P. T., Wood, M., Viola, K. L., and Klein, W. L. (2007) *J. Neurosci.* **27,** 796–807
17. Shankar, G. M., Bloodgood, B. L., Townsend, M., Walsh, D. M., Selkoe, D. J., and Sabatini, B. L. (2007) *J. Neurosci.* **27,** 2866–2875
18. Shankar, G. M., Li, S., Mehta, T. H., Garcia-Munoz, A., Shepardson, N. E., Smith, I., Brett, F. M., Farrell, M. A., Rowan, M. J., Lemere, C. A., Regan, C. M., Walsh, D. M., Sabatini, B. L., and Selkoe, D. J. (2008) *Nat. Med.* **14,** 837–842
19. Perrin, R. J., Fagan, A. M., and Holtzman, D. M. (2009) *Nature* **461,** 916–922
20. Walsh, D. M., and Selkoe, D. J. (2007) *J. Neurochem.* **101,** 1172–1184
21. Noguchi, A., Matsumura, S., Dezawa, M., Tada, M., Yanazawa, M., Ito, A., Akioka, M., Kikuchi, S., Sato, M., Ideno, S., Noda, M., Fukunari, A., Muramatsu, S., Itokazu, Y., Sato, K., Takahashi, H., Teplow, D. B., Nabeshima, Y., Kakita, A., Imahori, K., and Hoshi, M. (2009) *J. Biol. Chem.* **284,** 32895–32905
22. Ashe, K. H. (2001) *Learn Mem.* **8,** 301–308
23. Hardy, J., and Selkoe, D. J. (2002) *Science* **297,** 353–356
24. Klein, W. L., Stine, W. B., Jr., and Teplow, D. B. (2004) *Neurobiol. Aging* **25,** 569–580
25. Glabe, C. G. (2006) *Neurobiol. Aging* **27,** 570–575
26. Gösch, M., and Rigler, R. (2005) *Adv. Drug Deliv. Rev.* **57,** 169–190
27. Björling, S., Kinjo, M., Földes-Papp, Z., Hagman, E., Thyberg, P., and Rigler, R. (1998) *Biochemistry* **37,** 12971–12978
28. Bark, N., Földes-Papp, Z., and Rigler, R. (1999) *Biochem. Biophys. Res. Commun.* **260,** 35–41
29. Tjernberg, L. O., Pramanik, A., Björling, S., Thyberg, P., Thyberg, J., Nordstedt, C., Berndt, K. D., Terenius, L., and Rigler, R. (1999) *Chem. Biol.* **6,** 53–62
30. Pitschke, M., Prior, R., Haupt, M., and Riesner, D. (1998) *Nat. Med.* **4,** 832–834
31. Sengupta, P., Garai, K., Sahoo, B., Shi, Y., Callaway, D. J., and Maiti, S. (2003) *Biochemistry* **42,** 10506–10513
32. Provencher, S. W. (1982) *Comput. Phys. Commun.* **27,** 213–227
33. Provencher, S. W. (1982) *Comput. Phys. Commun.* **27,** 229–242
34. Palmer, A. G., 3rd, and Thompson, N. L. (1987) *Biophys. J.* **52,** 257–270
35. Walsh, D. M., Hartley, D. M., Kusumoto, Y., Fezoui, Y., Condron, M. M., Lomakin, A., Benedek, G. B., Selkoe, D. J., and Teplow, D. B. (1999) *J. Biol. Chem.* **274,** 25945–25952
36. Lomakin, A., Chung, D. S., Benedek, G. B., Kirschner, D. A., and Teplow, D. B. (1996) *Proc. Natl. Acad. Sci. U.S.A.* **93,** 1125–1129
37. LeVine, H., 3rd (1993) *Protein Sci.* **2,** 404–410
38. Tjernberg, L. O., Näslund, J., Lindqvist, F., Johansson, J., Karlström, A. R., Thyberg, J., Terenius, L., and Nordstedt, C. (1996) *J. Biol. Chem.* **271,** 8545–8548
39. Klein, W. L., Krafft, G. A., and Finch, C. E. (2001) *Trends Neurosci.* **24,** 219–224
40. Glabe, C. G. (2008) *J. Biol. Chem.* **283,** 29639–29643
41. Hepler, R. W., Grimm, K. M., Nahas, D. D., Breese, R., Dodson, E. C., Acton, P., Keller, P. M., Yeager, M., Wang, H., Shughrue, P., Kinney, G., and Joyce, J. G. (2006) *Biochemistry* **45,** 15157–15167
42. Bitan, G., Vollers, S. S., and Teplow, D. B. (2003) *J. Biol. Chem.* **278,** 34882–34889
43. Grant, M. A., Lazo, N. D., Lomakin, A., Condron, M. M., Arai, H., Yamin, G., Rigby, A. C., and Teplow, D. B. (2007) *Proc. Natl. Acad. Sci. U.S.A.* **104,** 16522–16527
44. Ono, K., Condron, M. M., and Teplow, D. B. (2009) *Proc. Natl. Acad. Sci. U.S.A.* **106,** 14745–14750
45. Bernstein, S. L., Dupuis, N. F., Lazo, N. D., Wyttenbach, T., Condron, M. M., Bitan, G., Teplow, D. B., Shea, J. E., Ruotolo, B. T., Robinson, C. V., and Bowers, M. T. (2009) *Nat. Chem.* **1,** 326–331
46. O'Nuallain, B., Freir, D. B., Nicoll, A. J., Risse, E., Ferguson, N., Herron, C. E., Collinge, J., and Walsh, D. M. (2010) *J. Neurosci.* **30,** 14411–14419
47. Chen, Y. R., and Glabe, C. G. (2006) *J. Biol. Chem.* **281,** 24414–24422
48. Sandberg, A., Luheshi, L. M., Söllvander, S., Pereira de Barros, T., Macao, B., Knowles, T. P., Biverstål, H., Lendel, C., Ekholm-Petterson, F., Dubnovitsky, A., Lannfelt, L., Dobson, C. M., and Härd, T. (2010) *Proc. Natl. Acad. Sci. U.S.A.* **107,** 15595–15600

SUPPLEMENTAL DATA

TWO DISTINCT AMYLOID β-PROTEIN (Aβ) ASSEMBLY PATHWAYS LEADING TO OLIGOMERS AND FIBRILS IDENTIFIED BY COMBINED FLUORESCENCE CORRELATION SPECTROSCOPY, MORPHOLOGY AND TOXICITY ANALYSES*

Satoko Matsumura, Keiko Shinoda, Mayumi Yamada, Satoshi Yokojima, Masafumi Inoue, Takayuki Ohnishi, Tetsuya Shimada, Kazuya Kikuchi, Dai Masui, Shigeki Hashimoto, Michio Sato, Akane Ito, Manami Akioka, Shinsuke Takagi, Yoshihiro Nakamura, Kiyokazu Nemoto, Yutaka Hasegawa, Hisayoshi Takamoto, Haruo Inoue, Shinichiro Nakamura, Yo-ichi Nabeshima, David B. Teplow, Masataka Kinjo, and Minako Hoshi

Additional Experimental Procedures

Amyloid β-protein (Aβ) and fluorescent probes- $A\beta_{1-40}$, $A\beta_{1-5}$, and $A\beta_{16-20}$ were synthesized using 9-fluorenylmethoxycarbonyl (FMOC) chemistry on an Applied Biosystems model 433A peptide synthesizer (1). Quantitative amino acid analysis, analytical HPLC, and matrix-assisted laser desorption ionization time-of-flight mass spectrometry (Ultraflex II, Bruker Daltonics) confirmed the structure and the purity of the peptides. The purified $A\beta_{1-40}$ was lyophilized, dissolved at 0.25 mM in 35% (v/v) acetonitrile (CH_3CN) in 0.1% (v/v) trifluoroacetic acid (TFA), and lyophilized (approximately 50 nmol/tube). This step was repeated twice. $A\beta_{1-42}$ (25 mg/ampoule) was purchased from Bachem (lots 0552992 and 1000255), dissolved completely in 50 ml of 1,1,1,3,3,3-hexafluoro-2-propanol (HFIP; Kanto Kagaku18529-1B) by incubating the peptide solution overnight at 4 °C and for another 3 hrs at 37 °C, and finally lyophilized (approximately 40 nmol/tube). The lyophilized peptides were kept at -20 °C. Fluorescent probes, $A\beta_{1-40}$ site-specifically labelled with tetramethylrhodamine (TMR) either at the N-terminus (NTR) or lysine 16 (K16TR), were synthesized using 6-carboxytetramethylrhodamine succinimidyl ester (Invitrogen). For NTR, γ-aminobutyric acid was attached to the $A\beta_{1-40}$ aspartic acid 1 using FMOC chemistry as described above. Before removing the side-chain protecting groups, γ-aminobutyric acid-conjugated $A\beta_{1-40}$ was labelled using succinimidyl ester of TMR through the primary amine. For K16TR, $A\beta_{1-40}$ was synthesized in a similar manner except that an acid-labile amine protecting group, *N*-[1-(4,4-dimethyl-2,6-dioxocyclohex-1-ylidene)ethyl] (Dde), was attached to the Nε-group of lysine at position 16. By removing the Dde with subsequent acid treatment, TMR was site-specifically attached to the lysine 16. The other side-chain protecting groups were finally removed from both NTR and K16TR by trifluoroacetic acid treatment. These fluorescent probes were purified (1), and their structure and purity were confirmed with quantitative amino acid analysis, analytical HPLC, and matrix-assisted laser desorption ionization time-of-flight mass spectrometry (Ultraflex II, Bruker Daltonics)(1). The probes were lyophilized, dissolved in 8% (v/v) CH_3CN in 0.1% (v/v) TFA, and lyophilized. After quantification by amino acid analysis (1), the probes were dissolved in 10% (v/v) CH_3CN in 0.1% (v/v) TFA, aliquoted in 500-μl Eppendorf microcentrifuge tubes (0.2-0.3 nmol/tube), and lyophilized. The lyophilized NTR and K16TR were kept at -20 °C.

Immunoprecipitations (IPs)- Previously we have shown that native-form ASPDs, equivalent to synthetic ASPDs, are present *in vivo* by immunoisolating them from soluble brain extracts of Alzheimer's patients using haASD1 antibody (2). As described previously (2), IPs with haASD1 were performed either using Immunocapturing Kit 100 MB-IAC Prot G (Bruker Daltonics) or using Protein Capturing Kit MB-CovAC-Select (Bruker Daltonics 254733) according to the manufacturer's instructions, except that bovine serum albumin (BSA) (final concentration of 3% (w/v); Sigma A7030) was used to suppress

non-specific binding as described previously (2). haASD1 or normal mouse IgG (control) was cross-linked to the protein G-magnetic beads. Since it has been shown that ASPDs exposed to Gentle Elution Buffer (GEB; ImmunoPure Gentle AgAb Elution buffer, pH 6.6; Pierce 21027) for 30-60 min retain their structure and toxicity (~100%) as determined using transmission electron microscopy (TEM) analysis, dot blotting using rpASD1, and toxicity assays (2), we conclude that a brief treatment of ASPDs with GEB would not have affected the ASPD structure. Therefore, captured ASPDs were eluted in GEB under neutral pH conditions. Immediately after elution, eluates were subjected to dot blot analysis using rpASD1, FCS measurements, and atomic force microscopy (AFM) observations. Eluates containing GEB were immediately exchanged to either F12 buffer without riboflavine, L-glutamine and phenol red (for toxicity assays) or a solution containing either 20 mM *N*-[tris(hydroxymethyl)methyl]-2-aminoethanesulfonic acid (TES), pH 7.5, 150 mM NaCl, and 1% fetal bovine serum (FBS) (for TEM observations) by three successive ultrafiltrations of the immunoprecipitation eluates using 50-kDa or 100-kDa MWCO filters (2). Recently, IPs with haASD1 have also been performed using Protein Capturing Kit MB-CovAC-Select (Bruker Daltonics 254733) according to the manufacturer's instructions, except that 3% (w/v) BSA was used to suppress non-specific binding as described above. In this case, captured ASPDs were eluted by the elution buffer, which was immediately neutralized to pH 7.5 with 100 mM phosphate buffer solution (pH 12.3). We confirmed that ASPDs retained their structure and toxicity by means of TEM, dot blotting, and toxicity studies as described above. The amount of ASPDs was determined using quantitative dot blot analysis or by amino acid analysis (1).

Dot Blotting- Samples diluted to the desired concentration in 100 µl PBS were blotted onto nitrocellulose membranes (PROTRAN 0.2 µm; Schleicher & Schuell) using a vacuum-blot apparatus (Biodot, Biorad). Membranes were washed three times with PBS, dried for 30 min at 37 °C, boiled for 5 min in PBS, and then blocked with 5% skim milk in Tris-buffered saline containing 0.05% (v/v) Tween 20 (TBS-T) for 1 hr at room temperature. Membranes were probed with rpASD1 (0.04 µg/ml) overnight at 4 °C, washed with TBS-T and incubated with appropriate horseradish peroxidase-conjugated secondary antibodies (highly cross-adsorbed anti-rabbit antibodies (1:7000), Zymed Laboratories) for 1 hr at room temperature. Immunoreactions were detected with SuperSignal West Femto chemiluminescent substrates (Pierce) and quantitated using a cooled CCD-based digital image analyzer LAS-1000 Plus (Fujifilm, Tokyo, Japan). The amount of purified ASPDs in IP eluates was determined from the standard curve of ASPDs prepared from $A\beta_{1-42}$ (0.03-4 pmol/dot, quantified by amino acid analysis) detected with rpASD1 antibody (0.04 µg/ml).

Transmission electron microscopy (TEM)- Samples were negatively stained with 4% (w/v) uranyl acetate solution on carbon-coated Formvar grids and then immediately analyzed using a JEOL JEM-1230 (BioScan) TEM at 100 kV assisted by an anti-contamination system using liquid nitrogen. Photography was done using a minimum-dose system to prevent radiation damage from the electron beam, as described previously (1). The images of ASPDs were captured at a direct magnification of 200,000 and the size of each spherical assembly was determined at the equator. Perfectly spherical assemblies of 10-15 nm diameter were counted as ASPDs, as described previously (1). The images of mature fibrils were captured at a direct magnification of 50,000. At least four fields were randomly selected in each preparation.

Fluid-phase imaging of ASPDs using atomic force microscopy (AFM)- Self-assembled monolayers (SAMs) of 11-amino-1-undecanethiol were freshly prepared on gold-coated mica substrates (Agilent Technologies, Palo Alto, CA) by immersing their surfaces in 5 mM ethanolic solution of 11-amino-1-undecanethiol (Dojindo Laboratories, Japan) overnight at room temperature, followed by

rinsing with ethanol and air-drying as described previously (3). The immunoisolated ASPDs (10 μl) were immediately deposited on the surface of the freshly prepared SAMs and left for 2 hrs, followed by rinsing twice with the ASPD preparation buffer (1). These samples were examined in the ASPD preparation buffer at room temperature using a multimode microscope with a Nanoscope III controller in a tapping mode fluid cell (Digital Instruments, Santa Barbara, CA) using a cantilever with a spring constant of 0.03 N/m (Olympus Corp.) (1). The height of ASPDs was obtained from the cross-sectional profile analyses of the AFM images (1), and a 0.5-nm width histogram was used to display the population. To determine the average height of each ASPD, we employed least-squares fitting (4) under the assumption that the size distribution of ASPDs showed a Gaussian profile (1). Since 2-3-nm structures were occasionally observed on SAMs, the size distribution of structures on SAMs was determined by least-squares fitting. However, in analyzing immunoprecipitated samples, these 2-3-nm structures were covered by the samples and were hardly detectable. Since the immunoprecipitation (IP) eluates contained 1% BSA (see IPs), the size distribution of substances in mouse IgG-IP eluates was determined as background. Finally, the size distribution of ASPDs in haASD1-IP eluates was determined under the assumption that haASD1-IP eluates contained both ASPDs and BSA-derived substances (used to block non-specific bindings in IPs), by least-squares fitting. There is no significant difference between the measured and least-squares-fitted data; the χ^2–statistics (degree of freedom) are 5.86 (39) for haASD1-IP eluates and 0.59 (19) for mouse IgG-IP eluates, respectively.

Fluorescence correlation spectroscopy (FCS)- FCS was performed with a confocal volume element of 0.3 femtoliters using a pre-production prototype apparatus (C10874; Hamamatsu Photonics K.K., Japan) equipped with a water immersion objective lens (UApo 40XW/340 NA=1.15; Olympus Corp.) as focusing optics. The confocal pinhole diameter was adjusted to 25 μm. TMR-labelled Aβ (NTR or K16TR) was excited with a DPSS laser (532 nm) at a CW output power of 100 μW (except for Supplemental Fig. S2). Fluorescent light emitted by TMR was collected by the above objective and separated from the excitation light (532 nm) by a dichroic mirror (540-nm beam splitter) and a 560-nm high-pass emission filter. Fluctuations in the fluorescence intensity were detected as photons using a photomultiplier tube (H7421) and the autocorrelation function was calculated using a digital correlator (M9003). Each sample (20 μl) was measured at room temperature for 3 sec x 10 times on an 8-well LaB-Tek Chambered Coverglass (155411; Nunc). Free rhodamine 6G (Sigma; 479 Da in mass, 2.8 x 10^{-10} m^2s^{-1} in D) or Alexa Fluor 532 C5 maleimide (Invitrogen; 813 Da, 2.8 x 10^{-10} m^2s^{-1}) was used as a reference to the confocal volume of the apparatus and to determine the mass or the diffusion coefficient of the sample using a program based on CONTIN (5,6).

FCS data evaluation- First, $G_{exp}(\tau)$ was calculated by averaging the autocorrelation function $G(\tau)$ of each FCS measurement, except for $G(\tau)$ of the measurements in which fluorescence bursts (derived from large insoluble probe aggregates or large fibrils) occurred, because such bursts distort $G(\tau)$. $G_{exp}(\tau)$ gives the distribution function $P(\tau_D)$:

$$G_{exp}(\tau) = 1 + A\int_0^{\infty} \frac{\theta(\xi - \tau_D)T_f(\tau) + \theta(\tau_D - \xi)T_s(\tau)}{\left(1 + \frac{\tau}{\tau_D}\right)\sqrt{1 + \frac{\tau}{s^2\tau_D}}} P(\tau_D)\, d\tau_D \qquad (1)$$

where τ_D is diffusion time, ξ is introduced as a parameter to classify τ_D into two groups (fast-diffusing assembly and slow-diffusing assembly) as described below, A is a constant, s is the structural parameter of the instrument set-up. $P(\tau_D)$ satisfies the following normalization condition,